Studies on the influence of solvothermally synthesized cerium metal ions doped $Li_4Ti_5O_{12}$ nanoparticles as anode materials for LIBs applications

Marie Rose Jesina Delavictoire[a], D. Muthu Gnana Theresa Nathan[a], S. John Sundaram[a], R. Mahesh[a], T. Manovah David[b], Shibu Joseph[a] and P. Sagayaraj[a*]

Abstract— The use of perfect electrode materials increases the demand for lithium ion batteries (LIBs) to spread wide in its application. Spinel $Li_4Ti_5O_{12}$ (LTO), by virtue of its various characteristic natures proves to be an important anode material. But the disadvantage of low conductivity limits its performance. This is overcome by the effect of metal doping. Hence in this paper efforts are made to dope LTO nanoparticles (NPs) with Cerium metal ions. The sample is prepared by a simple solvothermal approach employing Ce $(NO_3)_3.6H_2O$, TiO_2 and $LiOH.H_2O$ as raw materials. The samples were prepared with varying concentrations of the Ce dopant. The reaction was followed by high temperature calcination. The as-obtained CexLTO nanoparticles were characterized by Powder X-ray diffraction analysis (PXRD), Field Emission Scanning Electron Microscopy (FESEM) to determine the crystal structure and morphological features. The electrode materials Ce_xLTO formed by the substitution of Ce^{4+} ions are well crystallized and possess cubic spinel phase. An in-depth analysis on the growth of LTO nanoparticles was found from High Resolution Scanning Electron Microscopy (HRTEM) imaging. Energy Dispersive X-ray analysis (EDX) spectra analyses the elements present in the electrode material and the presence of vibrational groups are identified from Fourier Transform Infrared spectroscopy (FTIR) spectral data. Further electrochemical performance was studied through coin cell fabrication and the effect of dopant on the cyclic stability and discharge capacity of the Ce doped LTO is well investigated. The results show that Cerium metal ions doped LTO are more conductive compared to undoped LTO and hence could be directly used as efficient anode materials for LIBs.

Index Terms— Anode material, Ce-doping, Electrochemical study, Lithium-ion Batteries, Lithium Titanate nanoparticles, Solvothermal method.

1 INTRODUCTION

Nano-sized materials have emerged as attractive to bulk materials due to their various advantages of special electronic and chemical properties, which have aroused increasing interest among the researchers that could be used in the emerging field of electrochemical energy storage and thereby has also substantially expanded their use in electrodes for lithium batteries[1]. Rechargeable lithium-ion batteries (LIBs) with a high energy density and long lifetime are regarded as promising energy storage and conversion devices for application in electric vehicles (EVs) and smart grids. But the most commonly used graphite anode materials hinder the use of LIBs to deliver high capacity to large scale applications. Hence a wide range of alternate anode materials have been researched to satisfy the necessary requirements. In this regard $Li_4Ti_5O_{12}$ (LTO) is a promising anode material with many interesting characteristics like safety, zero-strain insertion behavior and high stability. The LTO anode can accommodate up to three lithium ions per formula unit, which allows a theoretical capacity of 175 mA h g^{-1} in the spinel structure [2], [3].

[a]*Department of Physics, Loyola College (Autonomous), Chennai- 600034, India*
[b]*Department of Chemistry, Madras Christian College (Autonomous), Chennai-600059, India*
E.Mail: psagayaraj@hotmail.com

The LTO electrode also shows a charge/discharge curve at a flat operating voltage of 1.55 V vs. Li^+/Li. This spinel-LTO is cheaper and easier to prepare than other alloy-based anodes, and has better electrochemical properties and better safety than carbonaceous anodes in LIBs [4], [5].

Since the oxidation state of Ti in spinel-LTO is the highest possible valence (+4), spinel-LTO is considered to be a very poor electronic conductor. Hence by doping a cation with a higher oxidation state into the tetrahedral 8a Li+ site or at the octahedral 16d Ti^{4+} site in the LTO anode, forces the partial transformation of Ti^{4+} into Ti^{3+} to generate a mixture (Ti^{3+}/Ti^{4+}) as charge compensation and increases the concentration of electrons. Doping with a variety of metal cations including Ag^+, Sn^{2+}, K^+, Mg^{2+}, Ca^{2+}, Zn^{2+}, Al^{3+}, Ga^{3+}, Cr^{3+}, Co^{3+}, La^{3+}, Y^{3+}, Zr^{4+}, Ru^{4+}, Mo^{4+}, Mn^{4+}, V^{5+}, Ta^{5+}, Nb^{5+}, Sr^{2+} and Cu^{2+} into the Li^+ and Ti^{4+} sites has been carried out and a detailed study owing to their structural and electrochemical behavior has been investigated earlier [6], [7], [8]. The observed results show the enhanced behavior exhibited electrochemically due to the substitution of metal ions in the crystal structure of LTO.

In this article doping of LTO by Ce^{4+} ions has been investigated employing solvothermal method. It is expected that the direct and fast transformation between Ce (III) and Ce (IV) enhances the electronic conductivity of the material. The as-

synthesized doped LTO nanomaterial is subjected to Powder X-ray Diffraction analysis (PXRD), Field Emission Scanning Electron Microscopy (FESEM), Energy dispersive X-ray analysis (EDX), High Resolution Transmission Electron Microscopy (HRTEM) and Fourier Transform Infrared Spectroscopy (FT-IR) studies. Further the electrical performance of Ce_xLTO has also been evaluated using CR2032 coin type cells.

2 Experimental Method

2.1 Chemicals

$LiOH.H_2O$ (99.995 % purity), $Ce(NO_3)_3.6H_2O$ (99.8 % purity) was purchased from Sigma Aldrich and Alfa Aesar. TiO_2 from Qualigens Fine chemicals Pvt. Ltd and Ethanol (99.9% AR grade) were purchased from Changshu Yangyuan Chemical Co., Ltd. These chemicals were used as received without further purification and the reactions were performed using de-ionized water (DI).

2.2 Synthesis of cerium doped LTO nanoparticles

LTO nanoparticles (NPs) were doped with Cerium using solvothermal method. The solvents namely ethanol and de-ionized water were mixed in equal volumes. 1.049 g of $LiOH.H_2O$ was first dissolved in the solvent mixture. The Cerium precursor was prepared with 0.3, 0.5 and 0.7 M% of Ce $(NO_3)_3.6H_2O$ dissolved in de-ionized water. To the dissolved LiOH aqueous solution, the above prepared Cerium solution was added and stirred. To which, a few grams of TiO2 was added finally and stirred for about an hour. The resultant white precipitate was transferred to a Teflon-lined stainless steel autoclave of 200 ml capacity. The hydrothermal synthesis was carried out at 200 °C for 12 h. After naturally cooling the autoclave to room temperature, the precipitate was separated by centrifugation. The obtained product was washed with DI water and ethanol several times, followed by drying and further calcination was done at 800 °C. The Ce doped LTO products were denoted as $Ce_{0.3}$LTO, $Ce_{0.5}$LTO and $Ce_{0.7}$LTO corresponding to the doping percentages of Cerium respectively. The same procedure was performed without the addition of Cerium precursor to obtain undoped LTO NPs

2.3 Electrochemical Measurement

The electrochemical performance of CexLTO (x= 0, 0.3, 0.5 and 0.7 M %) samples were tested in 2032 coin-type cells. Typically, Ce_xLTO, carbon black, and polyvinylidene fuoride (PVDF) with a weight ratio of 8: 1 : 1 were mixed in n-methyl pyrrolidinone (NMP) to form a uniform slurry, which was then coated onto a Cu foil substrate and dried in a vacuum oven at 120 °C for 12 h. Half-cells were assembled in a glove box using Li foil as counter electrode, Celgard 2300 as separator, and a mixture of 1 M $LiPF_6$ in ethylene carbonate and dimethyl carbonate (1 : 1 by volume) as electrolyte. The performance of the cells was evaluated galvanostatically in the voltage range of 1–2.5 V at a current rate of 0.1 C.

2.4 Characterization techniques

The as-synthesized Ce_xLTO products were characterized to analyze their structural, morphological, spectral and electrochemical behavior. The crystal structure, phase and crystallinity of the material was confirmed from Powder X-ray Diffraction (PXRD) analysis which was recorded with a GE XRD 3003 TTX-ray diffractometer using monochromatic Nickel filtered Cu Kα (λ = 1.5416 Å) radiation in the 2θ range of 10˚ to 70˚. The morphology, average size and elemental composition of the as-prepared nanoparticles were determined from the CARL ZEISS SUPRA 55 Field Emission Scanning Electron Microscopy (FE-SEM) that has the attachment of an Energy Dispersive X-ray Analyzer (EDX). This was further confirmed from High Resolution Transmission Electron Microscopy (HR-TEM) analysis done using the JEOL JEM 2100 and the selected area diffraction pattern (SAED) was also recorded to examine the crystallinity and phase formation of the as-synthesized nanoparticles. The FT-IR spectral analysis was obtained from the Perkin Elmer Spectrum RX 1. The electrochemical behavior was also carried out through coin cell fabrication.

3 Results and Discussion

3.1 Powder X-ray diffraction analysis

The crystal structure of Cerium doped LTO NPs were confirmed from Powder X-ray diffraction analysis. Fig. 1 shows the diffraction pattern corresponding to both LTO and cerium doped LTO with doping concentrations of 0.3, 0.5 and 0.7 M %. The diffraction peaks are compared with standard JCPDS (26-1198) and indexed to cubic spinel structure$Fd\bar{3}m$. The diffraction peaks are indexed to (111), (311), (400), (511) and (440) planes for all the three doping values which are the major planes of diffraction. There is not much difference in the intensity of (111) and (400) planes indicating the increased growth of the nanoparticles along these respective planes. Apart from the appearance of very less intense impurity peaks of Li_2TiO_3 and $LiTiO_2$, there are no other peaks seen, which clearly indicates that the cerium dopants have entered into the lattice sites of LTO without affecting the crystal structure of LTO.

Fig. 2 shows the expanded XRD plot for (111) peak. A shift towards the lower angles is observed with increase in doping concentrations when compared to undoped LTO. This indicates the increase in lattice constant due to the ionic radius of Ce^{4+} (0.87 Å) being larger than that of Li^+ (0.76 Å) and Ti^{4+} (0.605 Å). The lattice constant a=b=c is calculated to be 8.33 Å, 8.3505 Å, 8.3783 Å and 8.3499 Å for LTO, $Ce_{0.3}$LTO, $Ce_{0.5}$LTO and $Ce_{0.7}$LTO respectively. This increase in lattice constant due to the effect of doping could broaden the pathway for Li-ion diffusion and thus be more conductive to the insertion-extraction of Li-ions. Also the difference in the ionic radius between Ce^{4+} and Ti^{4+} creates lattice distortion leading to defects in LTO [9].

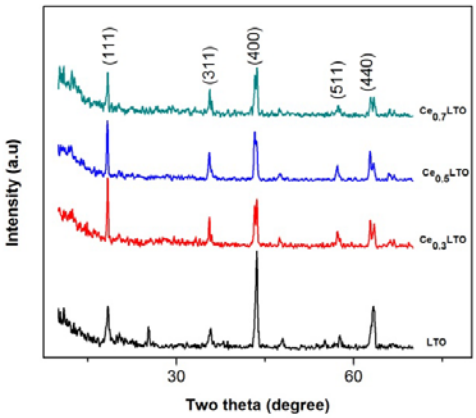

Fig.1. XRD pattern of Ce_xLTO NPs corresponding to x=0, x=0.3, x=0.5 and x=0.7

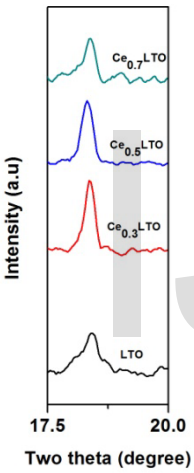

Fig.2. Diffraction peak of (111) expanded for varying concentrations of Ce_xLTO NPs

3.2 FESEM Analysis

The morphological study of Ce doped LTO was done using Field Emission Scanning Electron Microscopy (FESEM). Fig. 3 depicts the FESEM images of LTO, $Ce_{0.3}$LTO, $Ce_{0.5}$LTO and $Ce_{0.7}$LTO corresponding to the different doping concentrations. The Ce modified LTO NPs maintain the same cubic morphology and suggests no change in their shape owing to the increase in doping values. But at a high doping value of x= 0.7, the particles seem to have grown bigger and appear as bulk [10]. The increase in the calcination temperature from 500 °C to 800 °C could also lead to the formation of bigger particles compared to undoped LTO NPs. This is because the substitution of Ce^{4+} ions with greater radius for Ti^{4+} ions has resulted in lattice distortion leading to defects in LTO as observed.

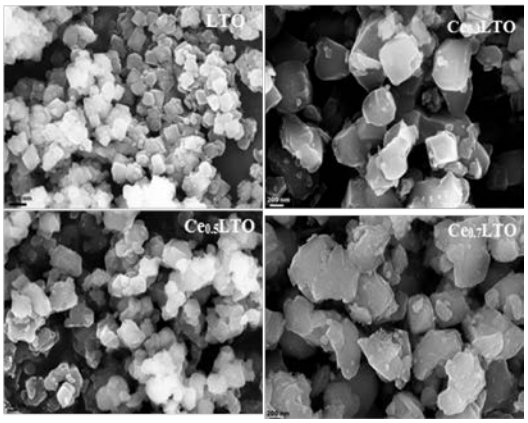

Fig.3. FESEM images of Ce_xLTO NPs for varying dopant concentrations

3.3 EDX Analysis

The Energy dispersive X-ray analysis (EDX) spectrum was recorded for all the as-synthesized Ce doped LTO nanoparticles. Fig.4 illustrates the EDX spectra corresponding to $Ce_{0.3}$LTO, $Ce_{0.5}$LTO and $Ce_{0.7}$LTO. From the spectra, the presence of titanium and oxygen were detected for the different doping concentrations. Added to this, the presence of cerium was detected. However, in the case of x= 0.3, its presence is not detected due to less doping additive of cerium [10]. But its presence is indicated for higher doping values of x= 0.5 and 0.7. Lithium, being a light metal produces low energy characteristic radiations and hence could not be detected from EDX analysis as observed in the case of undoped LTO nanoparticles. Hence requires other techniques like XPS or Li NMR to identify the presence of lithium [11].

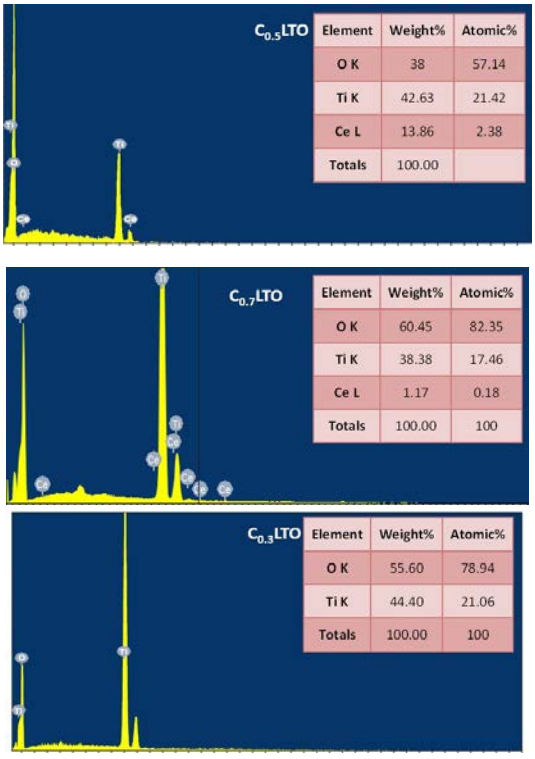

Fig.4. EDX spectra of Ce_xLTO NPs

3.4 HRTEM Analysis

A detailed study on the morphology and structural features of as-prepared Ce_xLTO NPs are observed from High resolution transmission electron microscopy (HRTEM). Fig. 5 (a-d) depicts the HRTEM images, selected area diffraction pattern (SAED) and lattice fringes obtained for various doping concentrations. As seen from FESEM analysis, the Ce_xLTO NPs are cubic in morphology. Owing to the increased doping values, the distortion in the shape of NPs is observed. The cerium doped LTO nanoparticles appear to be bulkier in size when compared to undoped LTO NPs. A clear examination on the microstructural information of lattice fringes was also analyzed. There occurs lattice distortion due to the substitution of Ce^{4+} with larger ionic radius in the site of Ti^{4+}, which has a comparatively smaller ionic radius as mentioned in XRD analysis. The typical selected area electron diffraction (SAED) patterns indicate that the nanoparticles are crystalline in nature. The d-spacing values are calculated from SAED analysis and compared with their corresponding XRD results and the major reflections are indexed to their respective diffraction planes. Thus the d-spacing values obtained from XRD and SAED patterns are indexed to the respective planes of (111), (311), (400), (511), (440) for $Ce_{0.5}$LTO and $Ce_{0.7}$LTO while, $Ce_{0.3}$LTO show major reflections from (111), (311), (400), (440) planes, thereby all three patterns confirm the spinel structure of the as-formed Ce_xLTO NPs.

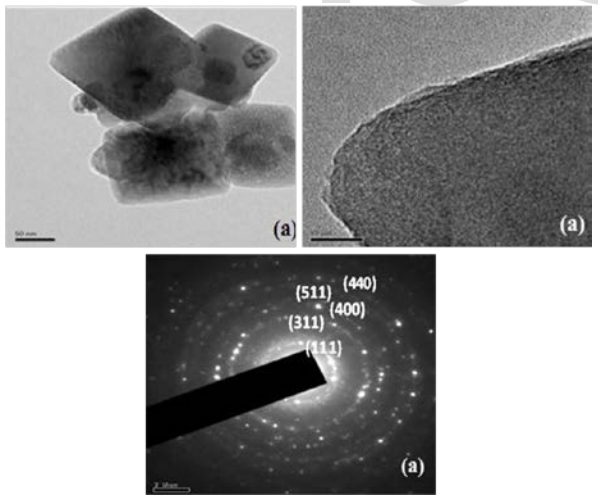

Fig.5. (a) HRTEM images, lattice fringes and SAED pattern of LTO NPs

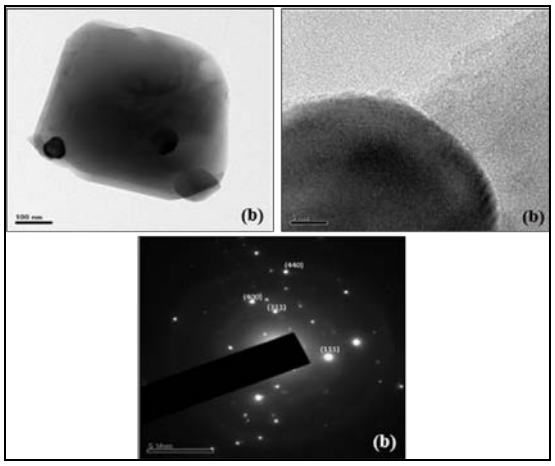

Fig.5. (b) HRTEM images, lattice fringes and SAED pattern of $Ce_{0.3}$LTO NPs

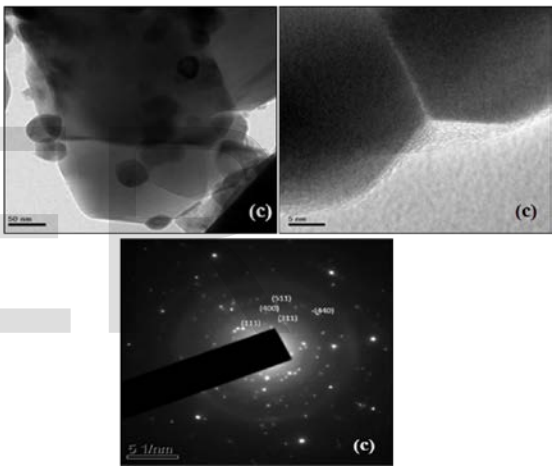

Fig.5. (c) HRTEM images, lattice fringes and SAED pattern of $Ce_{0.5}$LTO NPs

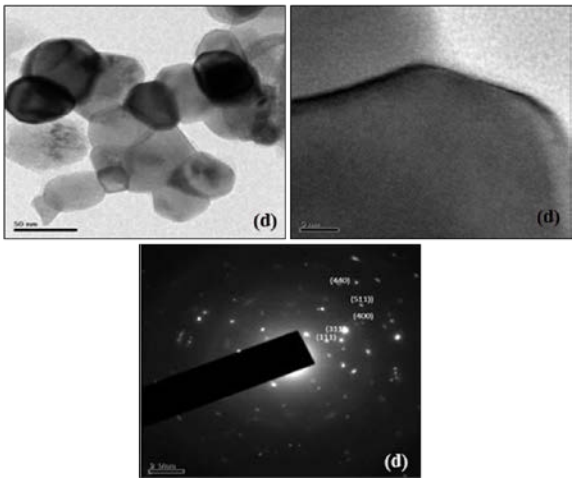

Fig.5. (d) HRTEM images, lattice fringes and SAED pattern of $Ce_{0.7}$LTO NPs

3.5 FTIR Analysis

The FT-IR spectra of the different Ce doped LTO samples are shown in Fig. 6. The spectra of all the three Ce_xLTO nanoparticles do not indicate major variation in the doping concentrations. The peak at about 3700 cm^{-1} indicates the presence of hydrogen-bonded O-H stretching in the Ce_xLTO structure [12]. The absorption bands in the range 1400- 1500 cm^{-1} correspond to C=O stretching vibrations. Thus two weak vibrations corresponding to the C=O stretching are observed, both seem to be nearly similar for $Ce_{0.3}$LTO, $Ce_{0.5}$LTO and $Ce_{0.7}$LTO i.e. one appears at about 1496 cm^{-1} and other at about 1438 cm^{-1} respectively [13]. Also the presence of C-O vibrations are confirmed from the bands at 1054.03 cm^{-1}, 1052.83 cm^{-1} and 1053.13 cm^{-1} for x= 0.3 , 0.5 and 0.7. The Ti-O vibrations are confirmed from the peaks observed between 2200- 2400 cm^{-1}, which are weak yet present in the spectra [15]. These bands are observed at 2394 cm^{-1}, 2399 cm^{-1} and 2395 cm^{-1} corresponding to $Ce_{0.3}$LTO, $Ce_{0.5}$LTO and $Ce_{0.7}$LTO. The bands lying below 600 cm^{-1} are considered to be due to the vibrations of the metal- organic groups, such as Li-O-R or Ti-O-R and Ce-O, this authenticates the presence of Cerium in the lattice sites of LTO [14].

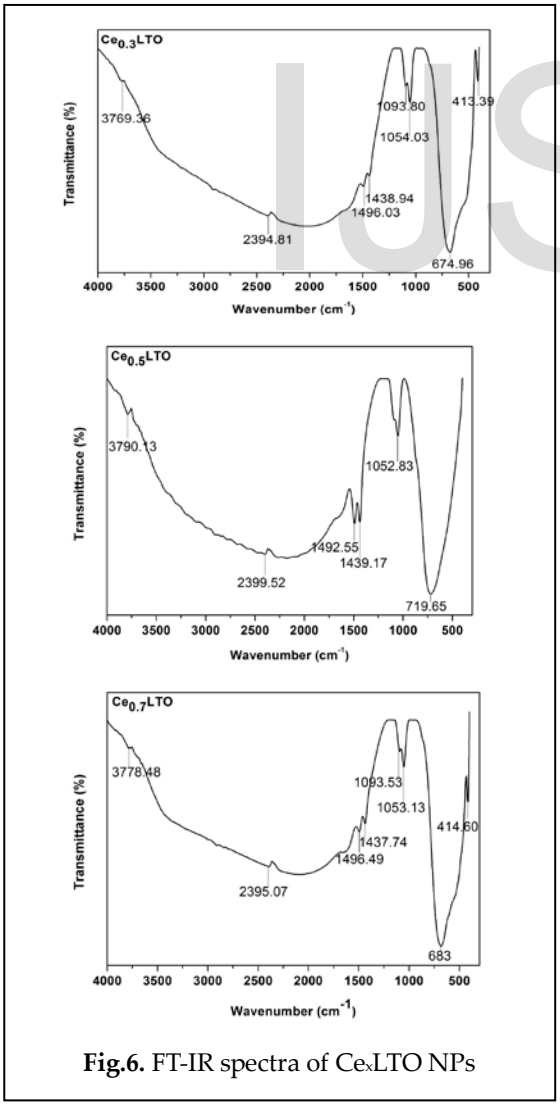

Fig.6. FT-IR spectra of Ce_xLTO NPs

3.5 Electrochemical Characterization

The electrochemical performance of Ce_xLTO nanoparticles was evaluated using CR2032 coin-type cells. Fig.7 illustrates the cycling behavior of Ce doped $Li_4Ti_5O_{12}$ nanoparticles obtained between 0 and 2.5 V (vs. Li/Li^+) at a C-rate of 0.1 C, was measured for 50 cycles. The lithiation and delithiation mechanism of $Ce_{0.5}$LTO, $Ce_{0.7}$LTO can be well understood from the charging/ discharging curves. Clear plateaus are found at about 1.54 V and 1.6 V for $Ce_{0.5}$ which lies nearly close to the theoretical two-phase reversible transition voltage plateau of 1.55 V versus Li^+/Li, implying good electro-activity of the sample at relatively low current density [16]. Whereas in the case of $Ce_{0.7}$, the voltage plateaus are not flat, and the corresponding potentials are found as 1.52 V and 1.66 V respectively [17].

As shown, an initial discharge capacity of 143.99 mAh g^{-1} for $Ce_{0.5}$ and 74.64 mAh g^{-1} for $Ce_{0.7}$ was delivered by the $Li_4Ti_5O_{12}$ electrodes. In the case of $Ce_{0.5}$LTO, a slight reduction in the discharge capacity was observed after the first cycle. However the $Ce_{0.5}$LTO electrode continues to maintain the capacity value at 117.71 mAh g^{-1} even at the end of 50th cycle. But whereas, in the case of $Ce_{0.7}$LTO, the discharge capacity falls below the initial value in the subsequent cycles and reaches a very low value of 31.78 mAh g^{-1}. Thus in this case, with increase in the doping content the capacity decreases. This occurs because as the content of dopants increase the molecular weight of LTO increases and thus its theoretical capacity decreases [18]. However their reversible reaction mechanism continues for all the 50 cycles unlike LTO where the electrochemical behavior ends within few cycles. It is notable that both the specific capacity values are lesser than the theoretical capacity (175 mAh g^{-1}). Hence comparing the behavior of Ce doped LTO NPs with LTO NPs, it is clear that $Ce_{0.5}$LTO shows better capacity than undoped LTO, while $Ce_{0.7}$LTO exhibits poor capacity.

These features indicate that $Ce_{0.5}$ doped LTO are more stable than LTO and show better electrochemical performance when compared to LTO. Hence it can be authenticated that doping Cerium particularly with x= 0.5 has enhanced the electrochemical performance and cyclic behavior of $Li_4Ti_5O_{12}$ NPs.

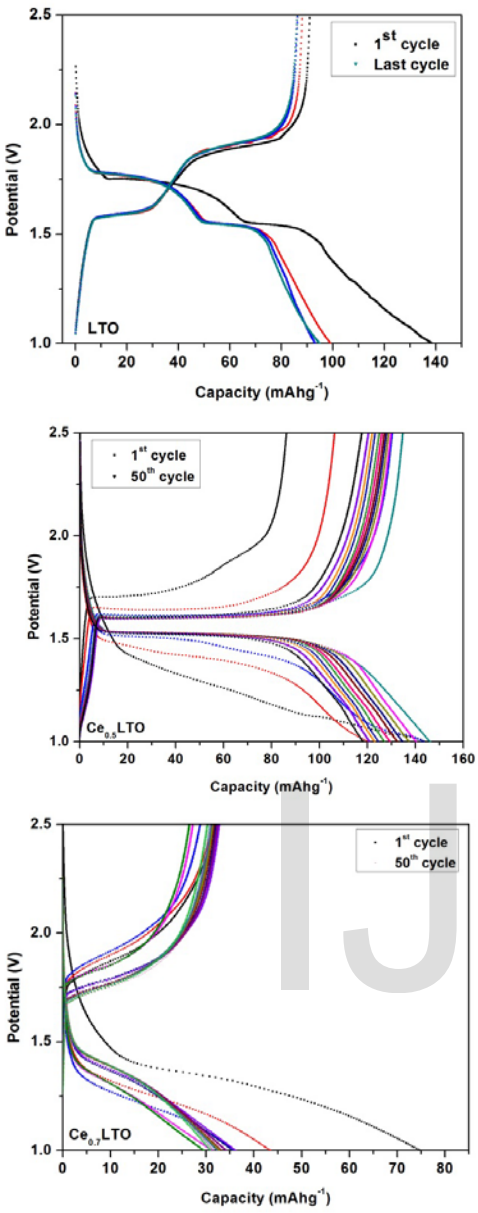

Fig.7. Charging-discharging behaviour of LTO, $Ce_{0.5}$LTO and $Ce_{0.7}$LTO NPs

4. Conclusion

Spinel $Li_4Ti_5O_{12}$ nanoparticles doped with Cerium metal ions have been successfully prepared by a facile, template free solvothermal method. Ce^{4+} ions are doped in the lattice site of titanium without changing the cubic crystal structure of LTO. The morphological aspect of the as-prepared Ce_xLTO nanoparticles was identified from FESEM characterization technique, which was further confirmed from the analysis of HRTEM imaging. With increase in doping content, the nanoparticles appear bigger with their shape slightly distorted. Also Ce_xLTO nanoparticles are found to be more conductive as observed from electrochemical analysis. They are also found to exhibit a reversible system. The doping content of x= 0.5 gives more stability and better discharge capacity to the material.

Acknowledgement

The authors acknowledge Loyola College-Times of India (LC-TOI) Research inititative (Ref.No.3LCTOI14PHY001) for funding this research work and for providing the research facility at Department of Physics, Loyola College (Autonomous), Chennai -600034. We also thank Dr. T. Prem Kumar, Senior Principal Scientist, CECRI, Karaikudi for helping us in carrying out the electrochemical study at his research lab and for the valuable discussions.

REFERENCES

[1] Arrebola J C, Caballero A and Hern´an L (2007), "High performance hybrid lithium-ion batteries based on combinations of nanometric materials", Nanotechnology, Vol. 18, pp. 295705-295709.

[2] Yonggang Wang, Huiqiao Li, Ping He, Eiji Hosono and Haoshen Zhou (2010), Nano active materials for lithium-ion batteries, Nanoscale, Vol. 2, pp. 1294-1305.

[3] Zhu G N, Yong-Gang W and Yong-Yao X (2012), "Ti-based compounds as anode materials for Li-ion batteries", Energy Environ. Sci., Vol. 5, pp. 6652-6667.

[4] Ding Z, Liang Z, Liumin S, Yang J, Sheng M, Yong-Sheng H, Zhaoxiang W and Liquan C (2011), "Towards understanding the effects of carbon and nitrogen-doped carbon coating on the electrochemical performance of $Li_4Ti_5O_{12}$ in lithium ion batteries: a combined experimental and theoretical study", Phys. Chem. Chem. Phys., Vol. 13, pp. 15127-15133.

[5] Sandhya, Bibin J and Gouri C (2014), "Lithium titanate as anode material for lithium-ion cells: a review", Ionics, Vol. 20, pp. 601-620.

[6] Gao J, Jierong Y, Changyin J and Chunrong W (2009), "Preparation and characterization of spherical La-doped $Li_4Ti_5O_{12}$ anode material for lithium ion batteries", Ionics, Vol. 15, pp. 597-601.

[7] Shenouda A Y and Murali K R (2008), "Electrochemical properties of doped lithium titanate compounds and their performance in lithium rechargeable batteries", J. Power Sources, Vol. 176, pp. 332-339.

[8] Chen C. H, Vaughey J T, Jansen A N, Dees D W, Kahaian A J, Goacher T and Thackeray M M (2001), "Studies of Mg-substituted $Li_{4-2x}Mg_xTi_5O_{12}$ spinel electrodes ($0 < x < 1$) for lithium batteries", J. Electrochem. Soc., Vol. 148, pp. A102-A104.

[9] Zhou T P, Feng X Y, Guo X, Wu W W, Cheng S and Xiang H F (2015), "Solid state synthesis and electrochemical performance of Ce-doped LTO anode materials for Li-ion batteries", Electrochim. Acta, Vol. 174, pp. 369-375.

[10] Chongling Cheng, Hongjiang Liu, Xin Xue, Shaomei Cao, Hui Cao and Liyi Shi (2014), Synthesizing nano-sized (~ 20 nm) $Li_4Ti_5O_{12}$ at low temperature for a high-rate performance lithium ion battery anode, RSC Adv.,Vol. 4, pp. 63105-63109

[11] Li H Y, Cheng D and Juan G (2008), "Hybrid microwave synthesis and characterization of the compounds in the Li–Ti–O system", J. Power Sources, Vol. 175, pp. 575-580.

[12] Lu J, Caiyun N, Qing P and Yadong L (2012), "Single crystalline lithium titanate nanostructure with enhanced rate performance for lithium ion battery", J. Power Sources, Vol. 202, pp. 246-252.

[13] Yu H Y, Ding Z, Zhi Z and Qi L (2014), "Thermal reactivity study of spinel lithium titanium oxide material for lithium ion battery by thermal and spectral analysis", J. Power Sources, Vol. 257, pp. 96-101.

[14]Chunming Z, Yaoyao Z, Jin W, Dan W, Dannong H and Yongyao X (2013), "$Li_4Ti_5O_{12}$ prepared by a modified citric acid sol-gel method for lithium-ion battery", J. Power Sources, Vol. 236, pp. 118-125.

[15]Yue L, Hailei Z, Zhihong T, Weihua Q and Xue L (2008), "Solvothermal synthesis and electrochemical characterization of amorphous lithium titanate materials", J. Alloys Compd., Vol. 455, pp. 471-474.

[16]Yujing S, Bote Z, Ran R, Rui C and Zongping S (2013), "Synthesis of well crystallized $Li_4Ti_5O_{12}$ nanoplates for Li-ion batteries with outstanding rate capability and cycling stability", J. Mater. Chem. A, Vol. 1, pp. 13233-13243.

[17]Li S, Jiaping W, Kaili J and Shoushan F (2014), "Mesoporous $Li_4Ti_5O_{12}$ nanoclusters as high performance negative electrodes for lithium ion batteries", J. Power Sources, Vol. 248, pp. 265-272.

[18]Chunfu Lin, Xiaoyong Fan, Yuelong Xin, Fuquan Cheng, Man On Lai, Henghui Zhou and Li Lu (2014) $Li_4Ti_5O_{12}$-based anode materials with low working potentials, high rate capabilities and high cyclability for high-power lithium-ion batteries: a synergistic effect of doping, incorporating a conductive phase and reducing the particle size, J. Mater. Chem. A, Vol. 2, pp. 9982-9993.